LIMNOLOGY
and
OCEANOGRAPHY

ASLO

Limnol. Oceanogr. 64, 2019, 650–660

doi: 10.1002/lno.11066

The role of double diffusion for the heat and salt balance in Lake Kivu

Tobias Sommer,[1] **Martin Schmid**,[1*] **Alfred Wüest**[1,2]

[1]Eawag, Swiss Federal Institute of Aquatic Science and Technology, Surface Waters - Research and Management, Kastanienbaum, Switzerland

[2]EPFL, École Polytechnique Fédérale de Lausanne, Physics of Aquatic Systems Laboratory, Margaretha Kamprad Chair, Lausanne, Switzerland

Abstract

Double diffusion in lakes and oceans can transform vertical gradients into staircases of convectively mixed layers separated by thin stable interfaces. Lake Kivu is an outstanding double-diffusive natural laboratory with > 300 such steps over the permanently stratified deep basin. Here, we use 315 microstructure profiles (225 measured in Rwanda and 90 in the DRC) to shed light on the heat and salt balances of Lake Kivu. Comparing profiles from 2011 and 2015 reveals warming of 8.6 mK yr^{-1} below 80 m depth and negligible changes in salinity. The double-diffusive layering is coherent over horizontal distances of 20–30 km and remained unchanged between 2011 and 2015, indicating little variability. The mean estimated dissipation within mixed layers is 1.5×10^{-10} W kg^{-1}. If unshaped Batchelor microstructure spectra are interpreted as nonturbulent, the rescaled dissipation of 0.44×10^{-10} W kg^{-1} corresponds to a vertical heat flux of 0.10 W m^{-2}, which agrees with the molecular heat flux through the adjacent stable interfaces. Using estimates of upwelling, temporal changes of temperature and salt, and vertical double-diffusive fluxes, we established heat and salt balances, which require lateral heat and salt inputs. For salt, lateral input of freshwater at the main gradients balances upwelling. For temperature, however, the divergence of the vertical double-diffusive fluxes can only be balanced by horizontal inputs supplying cool water above and warm water below the main gradients. This suggests that lateral inputs of water at various depths are the main drivers for this unique double-diffusive phenomenon in Lake Kivu.

Transport of heat, salt, nutrients, and various other particulate and dissolved substances is essential for the physical, biogeochemical, and ecological functioning of natural waters. Those transport rates in Lake Kivu are of particular interest, because it contains large amounts of dissolved methane (~ 60 km^3, at 0°C and 1 atm) and carbon dioxide (~ 300 km^3) in its deep-water layers (Schmid et al. 2005).

These gases, on the one hand, are a threat, because they could potentially trigger a limnic eruption (Schmid et al. 2003; Lorke et al. 2004) but, on the other hand, offer also an opportunity, as methane can be used as energy source. Since 2016, a first commercial-scale power station is operational, where deep water is syphoned to the lake surface, the dissolved methane is extracted, and the degassed water is reinjected to the deep water of the lake. Both Rwanda and the Democratic Republic of the Congo (DRC) intend to expand the use of this energy resource in the near future.

*Correspondence: martin.schmid@eawag.ch

Lake Kivu is further relevant from a fluid dynamics point of view, because it contains one of the most undisturbed signatures of double-diffusive layering in the world (Schmid et al. 2010; Sommer et al. 2013*a*; Fig. 1a, inset). In this work, we consider the vertical and horizontal structure of this double-diffusive layering to study the heat and salt balance of Lake Kivu. As the molecular diffusivities of salt and dissolved methane are similar, the results are also of high relevance for the initiated methane extraction (Schmid and Wüest 2012).

In Lake Kivu water, four agents determine water density, and all four increase with depth: temperature, salinity (both shown in Fig. 1a), methane, and carbon dioxide. As the stabilizing effect of salinity and carbon dioxide is larger than the destabilizing effect of temperature and methane, density is increasing with depth and the water column is gravitationally permanently stable below ~ 65 m depth (Schmid and Wüest 2012).

The large-scale vertical structure of temperature (Fig. 1a) and dissolved substances is shaped by the inflows of subaquatic groundwater discharge, which supplies water at various depths (Schmid et al. 2005; Ross et al. 2015). These intrusions contribute ~ 20% to the water balance of the lake (Muvundja et al. 2014). A small fraction of this groundwater

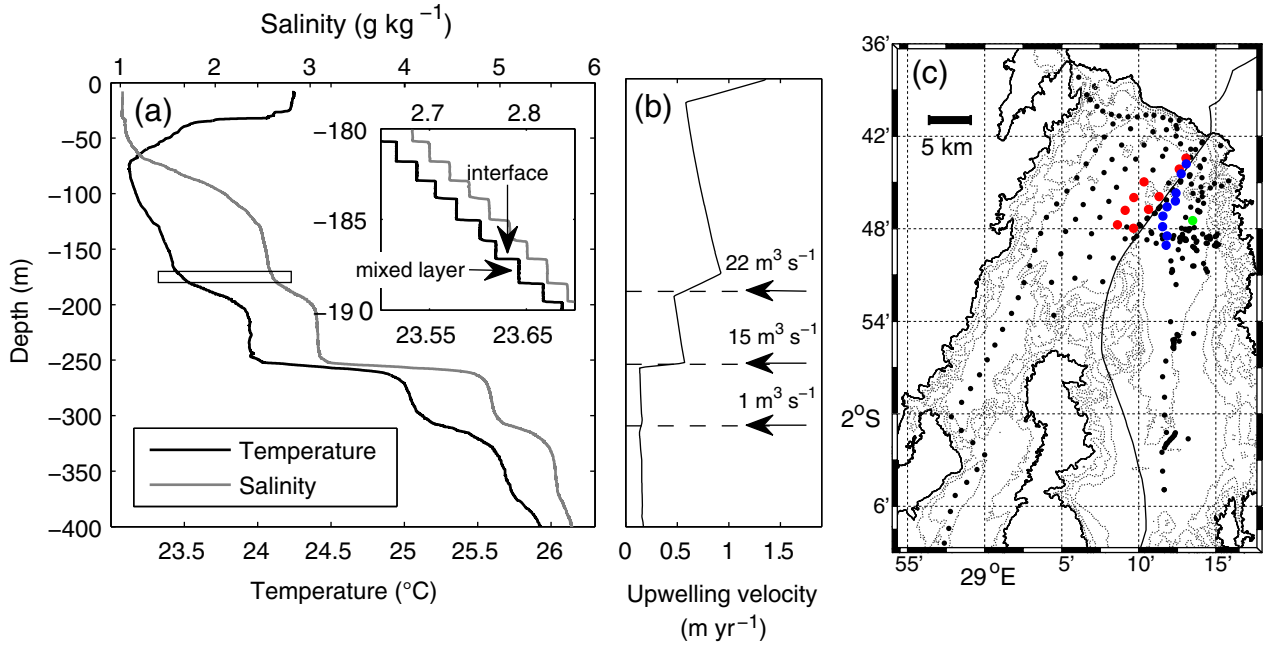

Fig. 1. Lake Kivu characteristics. **(a)** Vertical temperature and salinity profiles measured on 02 February 2011 at 13:30 at the location marked green in **(c)**. The box between 180 and 190 m depth indicates the depth interval of the inset with eight double-diffusive steps. **(b)** Upwelling velocity as used in the model of Schmid et al. (2005). The upwelling velocity is close to zero at the deepest location and its value increases stepwise toward the surface as water enters the Lake at various depths. The estimated discharges of the inflows are indicated above the horizontal arrows. The upwelling velocity decreases upward between individual water inflows because of the increasing Lake area toward the surface. **(c)** Profiling locations at Lake Kivu. Dots indicate the 315 profiles collected in 2010, 2011, and 2015. Blue and red dots indicate near-border profiles measured 2011 and 2015, respectively, that were used for estimating the warming rates in Lake Kivu. Bathymetric lines denote 100 m depth intervals; the thick line corresponds to the lake surface and the curved line is the border between Rwanda and the DRC.

discharge is composed of warm, saline water rich in carbon dioxide and mainly feeds the deep water below the main density gradient at 255 m depth. Most of the groundwater discharge is cooler and fresher and feeds the water column above the main gradient. A distinct groundwater source could be located at 250 m depth in the northern part of the lake and is responsible for maintaining the main density gradient just below this depth (Schmid and Wüest 2012; Ross et al. 2015). Other pronounced density gradients exist at ~ 190 and ~ 310 m depth, which are likely also maintained by the presence of inflows.

The groundwater discharge causes a slow upwelling (Fig. 1b) with estimated velocities and corresponding residence times of ~ 0.2 m yr^{-1} and ~ 800 yr below the main density gradient and up to ~ 1 m yr^{-1} and ~ 200 yr above the main density gradient. Upwelling is one of the transport mechanisms to remove heat and salt from the deep water. The other transport mechanism is small-scale diffusion. It includes both molecular and turbulent diffusion, and the latter is essentially double diffusion in Lake Kivu. Double diffusion enhances the vertical transport of water constituents (compared to molecular diffusion) by transforming gradual density gradients into staircases of convectively mixed layers, separated by thin stable interfaces (Fig. 1a, inset; Toffolon et al. 2015). Such staircases can develop when two agents that diffuse at different molecular rates contribute in opposing ways to the vertical density gradient (Schmitt 1994; Kelley et al. 2003; Radko 2013). In Lake Kivu, these two agents are mainly temperature and salinity. They both increase with depth, thus temperature is the destabilizing and salinity the stabilizing agent. Such a regime is the diffusive type of double diffusion, in contrast to the fingering type, where temperature and salinity decrease with depth (Kunze 2003; Schmitt 2003).

In the case of Lake Kivu, the dissolved gases also contribute to the density gradient. For the calculation of the density ratio, their density contributions are added to that of salinity based on their similar molecular diffusivities (Griffiths 1979; Schmid et al. 2004; Sommer et al. 2013*a*). The contribution to the density gradient by dissolved carbon dioxide is ~ 40% of the salinity density gradient (Schmid et al. 2003), and most of both the dissolved salts and carbon dioxide are assumed to enter the lake with the subaquatic groundwater discharge (Ross et al. 2015). Methane reduces the salinity density gradient by ~ 15%. It is partially of biogenic origin from the anaerobic decomposition of organic matter, while the remainder either stems from a direct source of geogenic methane or is produced by the reduction of carbon dioxide with geogenic hydrogen (Pasche et al. 2011).

In a previous study, we measured vertical fluxes of temperature and salinity through the double-diffusive staircases and

compared them to existing flux parameterizations of double diffusion (Sommer et al. 2013*b*). In another study, we used direct numerical simulations to show that molecular fluxes through interfaces are equal to the total vertical fluxes when the density ratio (the ratio of the stabilizing to the destabilizing vertical density gradient) is larger than three (Sommer et al. 2014).

In this work, we extend the 225 profiles used in previous publications and measured on the Rwandese side of Lake Kivu (Sommer et al. 2013*a*) by 90 new profiles on the Congolese side measured in 2015. With the Congolese profiles, we have now completed the data set of Lake Kivu covering evenly the entire deep part of the lake with profiling locations every ~ 2 km (Fig. 1c). We use these measurements to (i) determine warming rates in Lake Kivu; (ii) study the horizontal coherence of double-diffusive staircases; (iii) estimate dissipation rates of turbulent kinetic energy in the mixed layers; and (iv) relate these findings to the vertical diffusive heat fluxes. Finally, we combine warming rates and upwelling and vertical diffusive fluxes to form an overall heat and salt balance for Lake Kivu. Horizontal contributions are postulated to close the balance, and a comparison of the different terms in the heat and salt balance is used to derive conclusions on the interplay between subaquatic springs and double diffusion.

Methods

Microstructure measurements

Microstructure profiles of temperature and conductivity were measured with a free-falling Vertical Microstructure Profiler (VMP-500; Rockland Scientific International) at a descent rate of ~ 0.4 m s^{-1}. An algorithm was used to extract the temperature and salinity properties of double-diffusive interfaces and adjacent mixed layers from the combined standard and microstructure temperature and conductivity profiles. The algorithm is based on criteria relating small-scale gradients to background gradients and requesting approximate linearity in the interface core. Details of the algorithm, sensor specifications, sensor response corrections, as well as salinity and density calculations are found in Sommer et al. (2013*b*).

Dissipation rates of turbulent kinetic energy

To estimate turbulence levels, we determined the dissipation rates of turbulent kinetic energy ε by analyzing the vertical temperature microstructure signal within the double-diffusive mixed layers. The highly stable interfaces were excluded, as they are basically turbulence free (Sommer et al. 2013*a*). Dissipation rates were obtained by employing the maximum likelihood spectral fitting method (Ruddick et al. 2000; Steinbuck et al. 2009*a*) of the Batchelor spectrum S_B (Batchelor 1959; Gibson and Schwarz 1963) to the measured and frequency-response corrected temperature gradient spectrum, $S_{meas,}$ including the rejection criteria suggested by Ruddick et al. (2000). S_{meas} was obtained by first dividing the mixed layer into three equally long depth segments with 50% overlap. For each depth segment, the linear trend of the signal was subtracted and the gradient temperature spectrum computed. The three spectra were averaged and divided by the frequency response $\psi(f)^2$. The resulting spectrum is the spectrum S_{meas} used for Batchelor fitting.

The lower wavenumber limit for Batchelor fitting is set either by the length of the sampling interval or the upper bound of the inertial-convective subrange of turbulence (Steinbuck et al. 2009*b*), depending on which is larger. The upper wavenumber limit k_U for fitting depends on the frequency response of the FP07 thermistor as well as on the noise spectrum. The frequency response $\psi^2(f)$ (–) of the FP07 thermistors is given by $\psi^2 = (1 + [2\pi f\tau]^2)^{-2}$ with f (s^{-1}) being frequency and $\tau = 0.010$ s being the response time (Sommer et al. 2013*b*). Requiring that $\psi^2(f) > 0.1$ sets the upper frequency limit to $f_U = 23$ Hz and thus $k_U = 2\pi\ f_U/W$ (rad m^{-1}) with W (m s^{-1}) being the sinking speed of the VMP-500 profiler. The noise spectrum $S_{ns}(f)$ (K^2 s) was approximated by $S_{ns}(f) = 10^b f^m$ with $m = -0.6962$, $b = -10.5503$ for profiles measured in 2010 and 2011 (f in units of s^{-1}) and, because of a change in the electronic circuit, using $m = -0.3925$, $b = -10.9749$ for profiles measured in 2015. We validated the noise spectra by lab bench measurements and field observations at weak turbulence. Requiring that S_{meas} exceeds S_{ns} by at least a factor of two may eventually decrease k_U further.

To estimate the uncertainty of the microstructure methods is challenging as there are, besides the accuracies of the sensors, unknown biases, which partly depend on the nature of the sampled turbulent flow (Steinbuck et al. 2009*b*; Gregg et al. 2018) and the intrinsic intermittency of turbulence in stratified natural waters of at least one order of magnitude. Therefore, in most microstructure studies, the focus is on spatial structures or temporal dynamics, and absolute accuracies are not reported. As shown below (Dissipation Rates and Vertical Structure of the Heat Fluxes section), a large fraction of evaluated depth segments produce unshaped Batchelor spectra, probably caused by the intermittency in this particular low-turbulence environment. Those unshaped spectra cannot be evaluated and cause a large absolute uncertainty. Even though in another study, a comparison of more than 70,000 parallel temperature- and shear-based dissipation estimates revealed agreements of better than a factor of two (15% difference of the averages; Kocsis et al. 1999), we interpret here only the vertical structure of the dissipation.

Vertical diffusive heat and salt fluxes

Vertical diffusive heat fluxes in Lake Kivu were estimated using two methods. The first method is based on molecular fluxes through double-diffusive interfaces (Sommer et al. 2013*a*). The vertical diffusive temperature flux F_{Tz} (K m s^{-1}) is defined by $F_{Tz} = -\kappa_T \partial T/\partial z|_{int}$, where $\kappa_T = 1.4 \times 10^{-7}$ m^2 s^{-1} is the molecular diffusivity of heat at deep-water temperatures and $\partial T/\partial z|_{int}$ is the measured vertical temperature gradient within double-diffusive

interfaces (Sommer et al. 2013*b*) (z decreases in the downward direction). The corresponding heat flux, F_H (W m^{-2}), is then given by $F_H = c_p \rho F_{Tz}$ with specific heat capacity c_p (J kg^{-1} K^{-1}) and water density ρ (kg m^{-3}).

The second method for estimating vertical diffusive heat fluxes $F_{H\varepsilon}$ is based on measured ε and assumes mechanical energy conservation (i.e., potential plus kinetic energy) within the double-diffusive layers (Hieronymus and Carpenter 2016). The buoyancy flux J_{int} through a double-diffusive interface is equal to the dissipation rate ε within the mixed layer plus a diffusive buoyancy flux J_d within the mixed layer (for derivation see Hieronymus and Carpenter [2016]):

$$J_{int} = \varepsilon + J_d \tag{1}$$

The ratio $\gamma_H \equiv J_d/J_{int}$ of the two buoyancy flux terms is ~ 0.20 for a mixed-layer-based Rayleigh number of ~ 10^8 typical for Lake Kivu (Sommer et al. 2014; Hieronymus and Carpenter 2016). Using this definition for γ_H leads to a relation to the measured dissipation ε by

$$J_{int} = \frac{\varepsilon}{1-\gamma_H} \tag{2}$$

The interfacial buoyancy flux is defined by

$$J_{int} = \frac{\alpha g}{c_p \rho} F_{H\varepsilon} - R_f \frac{\alpha g}{c_p \rho} F_{H\varepsilon} \tag{3}$$

Here, α (K^{-1}) is the thermal expansion coefficient, g is the gravitational constant (m s^{-2}), and R_f (–) is the double-diffusive flux ratio, which is the ratio of the salt flux-driven buoyancy flux to the heat flux-driven buoyancy flux. Here, we use $R_f = 0.11$ corresponding to the average flux ratio measured in Lake Kivu (Sommer et al. 2013*a*). Combining Eqs. 2 and 3 leads to a formulation for calculating $F_{H\varepsilon}$.

$$F_{H\varepsilon} = \frac{1}{(1-R_f)(1-\gamma_H)} \frac{c_p \rho}{g\alpha} \varepsilon \tag{4}$$

The vertical salt fluxes F_{Sz} (g kg^{-1} m s^{-1}) are calculated from F_{Tz} using $F_{Sz} = (\alpha/\beta) R_f F_{Tz}$, where β (kg g^{-1}) is the haline contraction coefficient.

In order to relate the vertical diffusive fluxes to the vertical background gradients of temperature and salinity, we define a vertical apparent diffusivity, which for temperature is $\kappa_{Ta} = -F_{Tz}/(\partial T/\partial z)$ and for salinity $\kappa_{Sa} = -F_{Sz}/(\partial S/\partial z)$. Here, $\partial T/\partial z$ and $\partial S/\partial z$ are the background gradients (calculated by linear fits over consecutive vertical intervals of 2 m) of temperature and salinity, respectively.

The lower theoretical limit for the vertical diffusive heat and salt flux is given by molecular diffusion through the background gradient and is defined by $F_{H,mol} = -c_p \rho \kappa_T \partial T/\partial z$ and $F_{S,mol} = -\kappa_S \partial S/\partial z$, respectively. Here, $\kappa_S = 1.43 \times 10^{-9}$ m^2 s^{-1} is the combined diffusivity of salt, methane, and carbon dioxide (Sommer et al. 2013*a*).

Results and discussion

Warming of Lake Kivu

In order to determine temperature and salinity changes in Lake Kivu over time, we chose 18 profiles of temperature and salinity close to the border of Rwanda and the DRC. Nine of these were measured in 2011 in Rwanda (marked blue in Fig. 1c) and nine in 2015 in the DRC (marked red in Fig. 1c). We then averaged the temperature profiles (Fig. 2a) measured in 2011 and 2015, respectively, and calculated the rate of change from their difference (Fig. 2b). The profiles selected that way are all located in the open water of the northern basin and are chosen as close to each other as possible, while reaching down to a depth of at least 375 m. By this, we ensure that temperature profiles are compared with minimal spatial bias. Additionally, we calculated temperature trends from 2002 to 2018 from an independent set of six temperature profiles measured in the years 2002, 2004, 2007, 2010, 2012, and 2018 within the same area. The profiles show a consistent temperature increase at all depths. Below 80 m depth, Lake Kivu has been warming at an average rate of 8.6 mK yr^{-1} between 2011 and 2015 and at a rate of 10.4 mK yr^{-1} between 2002 and 2018 (Fig. 2b). Above the main density gradient, the warming rate increases upward from ~ 5 mK yr^{-1} at 225 m depth to ~ 19 mK yr^{-1} at 80 m depth in agreement with previous warming trends from 1975 to 2004 and 2004 to 2011, which were extracted from fig. 5a in Katsev et al. (2014). At 350 m depth, we observed a similar trend as found by Katsev et al. (2014) for the period from 2004 to 2011. This recent warming of 10–15 mK yr^{-1} was absent in the trend from 1975 to 2004. At 285 m, we determined a warming rate of ~ 3 mK yr^{-1} for 2011 to 2015 and ~ 10 mK yr^{-1} for 2002 to 2018, which are both smaller than the 14 mK yr^{-1} determined by Katsev et al. (2014) from 2004 to 2011 but similar to the trend from 1975 to 2004.

The observed warming rates of 8.6 and 10.4 mK yr^{-1} are similar to other great African Lakes (O'Reilly et al. 2003; Verburg et al. 2003). In these lakes, warming is explained by increased surface water temperatures caused by climate warming and subsequent downward transport of heat by turbulent diffusion. In Lake Kivu, however, turbulence is suppressed by the extraordinarily stable stratification indicated by the existence of double-diffusive layering, and the warming of the deep water (> 80 m depth) thus cannot be explained by heat input from the surface (Katsev et al. 2014). Rain water, which infiltrates into volcanic fissures on land and enters the lake below the surface, may, however, carry the atmospheric warming signature to the deep water of Lake Kivu. We plan to investigate this hypothesis by age measurements of the water using ^{39}Ar as age tracer. Also, the anaerobic decomposition of organic matter into methane and carbon dioxide releases heat into the lake water. Based on the carbon and methane budgets

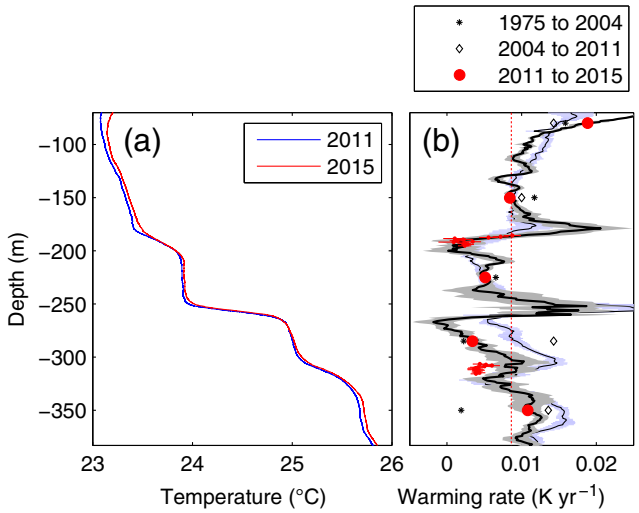

Fig. 2. Warming rates of Lake Kivu. **(a)** Averaged temperature profiles from 2011 (blue) and 2015 (red), respectively, measured at the locations indicated in Fig. 1c. **(b)** Warming rate (black line) determined from the difference of the two profiles in **(a)**. The gray shading indicates the standard error of the black line calculated from the standard errors of the averaged profiles. The large red dots were obtained by averaging the black line over a depth interval of 1 m centered at the red dots. The blue line shows warming rates estimated from six independent temperature profiles measured between 2002 and 2018, including standard error of the trend from linear regression. Black stars and diamonds indicate warming rates determined by Katsev et al. (2014) for 1975 to 2004 and 2004 to 2011, respectively. The red dashed line indicates the mean warming rate of 8.6 mK yr^{-1} below 80 m depth calculated from the black line. The small red dots (with error bars) at 190 and 310 m depth were obtained from the temperatures differences of the coherent mixed layers shown in Figs. 3b,d.

estimated by Pasche et al. (2011) and the heat release for acetoclastic and hydrogenotrophic methanogenesis (Fey and Conrad 2000), this heat release corresponds to a warming rate of ~ 2.4 mK yr^{-1} below the main gradient at 255 m depth and 0.10 mK yr^{-1} above. However, assuming that the current temperature is in steady state with the long-term average organic matter decomposition, only the contribution of the recent increase in methane production (i.e., about one third of the current production) should contribute to the observed heating. Thus, we can expect that realistically not more than a fraction of ~ 10% of the apparent warming of 8.6 mK yr^{-1} below the main gradient is of biogenic origin. Temperature sensor accuracies and drifts do not influence our measurements by more than ~ 10%, because the same well-aged (more than 10-yr old) SeaBird SBE-3F sensor was used in 2011 and 2015 for which we never had to correct readings after cross calibration in a Hart bench-top calibration bath. This indicates a drift of less than 1 mK yr^{-1} or ~ 10% of the observed temperature trends. Moreover, two independent measurements with different sensors, that is, our profiles from 2002 to 2018 and the profiles from 1975 to 2014 (Katsev et al. 2014), yielded comparable temperature trends and thus corroborate the warming trend observed between 2011 and 2015. However, the reason for the exceptionally large warming rate of > 10 mK yr^{-1} below 340 m depth (Fig. 2b) remains unclear and should be monitored in the future to be aware of a potential destabilization of the water column.

Horizontal coherence of the layering

Horizontal coherence of the layering was studied by extracting salinities and potential temperatures from mixed layers for profiles measured at different locations (Schmitt et al. 1987; Timmermans et al. 2008; Polyakov et al. 2012; Scheifele et al. 2014; Meccia et al. 2016). A clustering in temperature–salinity space is interpreted as a signature of horizontal coherence. In Lake Kivu, we observed such clustering especially between 185 and 196 m and between 306 and 316 m depth (Fig. 3a,b,d). To identify those clusters easily, they are framed by gray boxes in Fig. 3b,d. Clusters identified in the profiles of 2011 connect seamlessly to clusters measured in 2015 indicating surprisingly small temporal variability of the double-diffusive staircase structures over the 4-yr period. Coherent mixed layers measured in 2015 (red dots in Fig. 3b,d) show increased temperatures compared to mixed layers measured in 2011 (blue dots in Fig. 3b,d) but almost no changes in salinity. This underpins the warming trend determined from the averaged profiles in Fig. 2. In order to investigate the horizontal coherency of mixed layers, we focused on one cluster at 190 and one at 310 m depth (framed in green in Fig. 3b, d). For each dot in these clusters, the profiling location was extracted and plotted in Fig. 3c,e with the color indicating the temperature of the mixed layer at each location. The mean temperature difference between 2011 and 2015 was subtracted from the temperatures measured in 2015 to get a purely spatial pattern. At 190 m depth, the mixed layers are coherent over almost the entire northern basin (Fig. 3c). A cold signature of water entering the lake from the northern shore is identified, in agreement with observations by Ross et al. (2015), and can be followed south for ~ 5 km along the Rwandan-Congolese border (black line in Fig. 3c,e). Coherent layers at 310 m depth (Fig. 3e) are also present; however, in comparison to 190 m depth, they are located further away from the northern shore and extend ~ 20 km into the south-eastern branch of Lake Kivu. Horizontal variations of temperature, both at 190 and 310 m depth, are ~ 0.10°C.

Dissipation rates and vertical structure of the heat fluxes

Dissipation rates ε (W kg^{-1}) of turbulent kinetic energy indicate turbulence levels and provide an independent estimate for the vertical diffusive heat fluxes. The distribution of ε is shown in Fig. 4a. Measured dissipation rates are close to log-normally distributed, but for unknown reasons, the set of ε estimates contains some very large (> 10^{-7} W kg^{-1}) and small (< 10^{-12} W kg^{-1}) values, and therefore, the kurtosis of the logarithmic data is 4.3 instead of the expected value of 3.0 for a normal distribution. Consequently, the distribution fails the Lilliefors test for normality. In principle, this could be avoided by removing the ~ 50 largest and smallest values, which

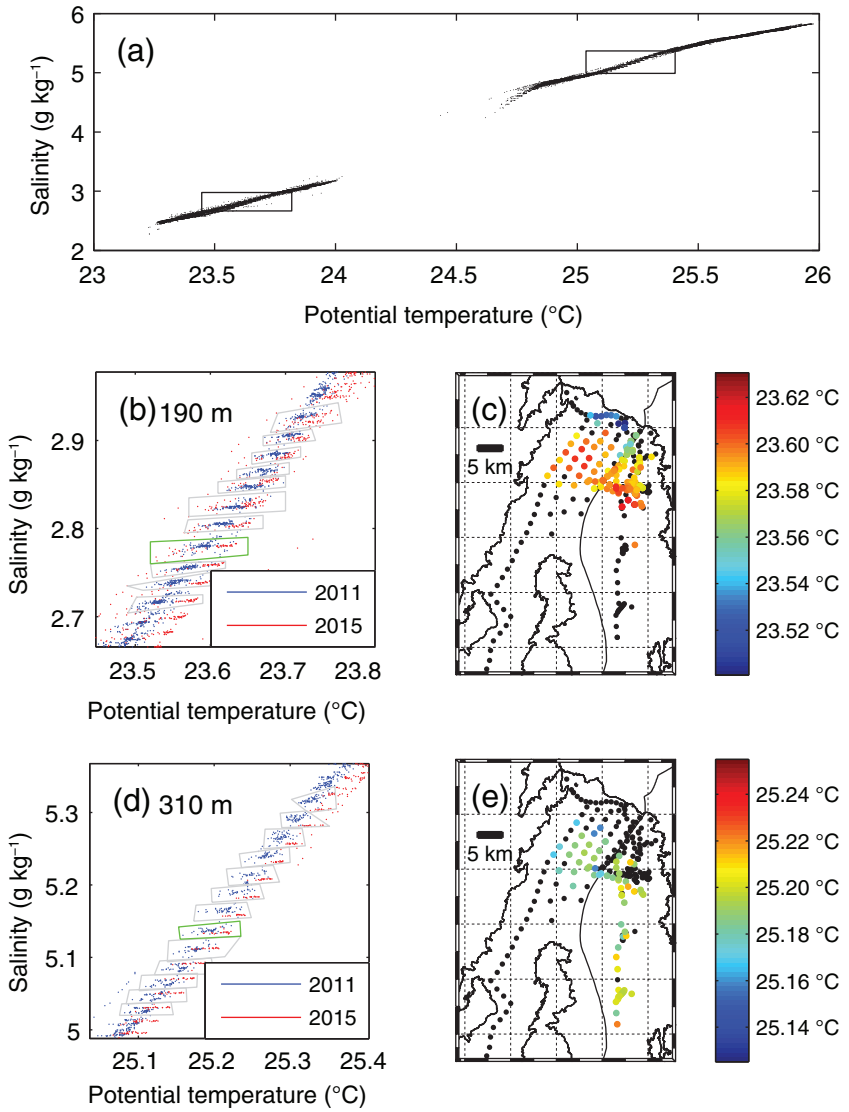

Fig. 3. Horizontal coherence of the double-diffusive layering. **(a)** Salinities plotted against potential temperatures for all mixed layers measured in 2011 and 2015. **(b, d)** Enlarged section of coherent mixed layers indicated by the two frames in **(a)**. The gray frames in **(b, d)** are drawn manually around coherent clusters. **(c, e)** Potential temperature maps of the mixed layers enveloped by the green frames in (**b** and **d**), respectively. The solid black line indicates the Rwandan-Congolese border. In **(c, e)**, the warming rates were subtracted from the profiles measured in 2015 in order to obtain a purely spatial temperature representation.

results in a perfectly lognormal distribution of the remaining values. However, as there are no arguments to remove extreme values, we decided to keep the entire data set and estimate the mean using the maximum likelihood estimator of a lognormal distribution, which is 1.5×10^{-10} W kg^{-1} (Fig. 4a). This is a better estimate for the true mean than the arithmetic mean (3.0×10^{-10} W kg^{-1}), which is strongly affected by few extremely large values. The standard deviation of the log-transformed data is 1.61, corresponding to a factor of 5.0 after back-transformation. Unfortunately, the effective mixed layer average of ε carries a large error, because 70.4% of the microstructure segments did not show Batchelor-type forms. These were rejected for ε estimation and are therefore missing in the average of 1.5×10^{-10} W kg^{-1}. We consider too weak turbulence, unable to produce Batchelor-like spectra, as the most probable reason for rejection. The inspection of numerical simulations of convective turbulence, as presented in fig. 1b in Gayen et al. (2013) and fig. 2b in Sommer et al. (2014), indicate large regions within the mixed layer which are distant to the main shearing zones related to the driving plumes. Assuming such strong inhomogeneity in dissipation and setting all rejected ε estimates to zero would provide a mixed layer average of 0.44×10^{-10} W kg^{-1}.

Figure 4b shows two histograms of the related vertical diffusive heat fluxes, either estimated from ε ($F_{H\varepsilon}$) or from molecular fluxes through the double-diffusive interfaces (F_H). The mean of

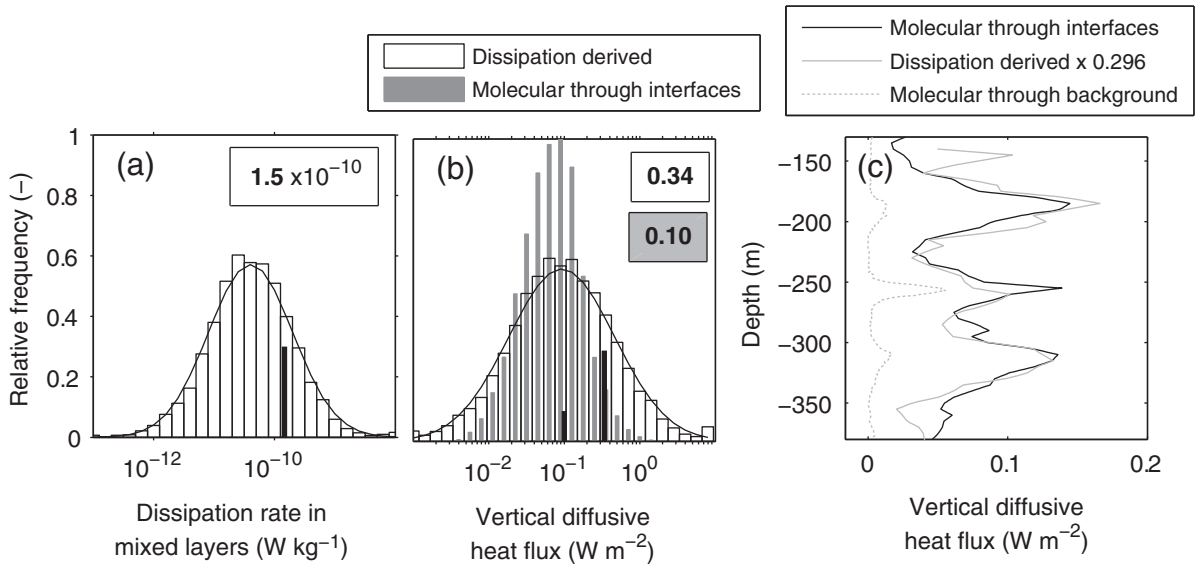

Fig. 4. Dissipation rates and vertical diffusive heat fluxes. **(a)** Histogram of the dissipation rate of turbulent kinetic energy in the mixed layers (n = 9408). The maximum likelihood estimator (mle) of the mean of 1.5×10^{-10} W kg^{-1} is indicated by the black vertical bar. The black curve is the probability density function of the corresponding lognormal distribution. **(b)** Histogram of vertical diffusive heat fluxes calculated from the dissipation rates in **(a)** (white bars, n = 9408). The mle of the mean is 0.34 W m^{-2}, indicated by the right black vertical bar. For comparison, the vertical diffusive heat fluxes calculated from molecular fluxes through interfaces are superimposed in gray (arithmetic mean and mle of the mean are both 0.10 W m^{-2}, n = 13,971). **(c)** Vertical structure of the vertical diffusive heat flux. Heat fluxes were first binned into depth segments of 10 m with 50% overlap, and for each bin, the mle of the mean was calculated and plotted. Note that the dissipation-derived heat flux is rescaled by multiplying with 0.296 for comparison with the interfacial flux. The molecular flux through the background gradient is also shown for comparison (dotted line).

the estimates of the ε-derived heat fluxes is 0.34 W m^{-2} (Fig. 4b). If rescaled with a factor of 1–0.704 = 0.296, which accounts for the 70.4% rejected spectra as zero dissipation, the mixed layer average is 0.10 W m^{-2}. For F_H, for which all estimates are valid and therefore to 100% included in Fig. 4b, the arithmetic mean and the maximum likelihood estimate are equal at 0.10 W m^{-2} and also in agreement with Sommer et al. (2013*a*) for measurements on the Rwandan side only. The standard deviation of the log-transformed data is 0.90, corresponding to a factor of 2.5 after back-transformation. Although the numerical coincidence of the mixed layer averages of F_H, and the rescaled $F_{H\varepsilon}$ is accidental at 0.10 W m^{-2} (Fig. 4b), it indicates that the interpretation of the dissipation values is consistent. For the following heat balance calculations, we, however, exclusively use F_H (or the corresponding temperature flux F_{Tz}), as F_H is based on molecular fluxes through interfaces and has been shown to well capture the total fluxes (Sommer et al. 2014).

The depth dependence of F_H and $F_{H\varepsilon}$ as well as $F_{H,mol}$ is shown in Fig. 4c with a vertical binning resolution of 10 m. F_H exceeds molecular fluxes by factors of 10 to 60 and is largest ($F_H \approx 0.15$ W m^{-2}) near the centers of the main gradients at 190, 255, and 310 m depth. The structure of $F_{H\varepsilon}$ (scaled by a factor of 0.296) follows astonishingly well the structure of F_H and thus independently confirms the structure (not the magnitude) of the observed heat flux variations (Fig. 4c). Although, as mentioned above, we have no concluding proofs that 70.4% of the microstructure segments are nonturbulent, the match between F_H and 29.6% of $F_{H\varepsilon}$ (Fig. 4c) supports the hypothesis that the rejected microstructure segments are of very low turbulence levels.

Heat and salt balance

We combine our measurements to form a heat and salt balance for the water column of Lake Kivu and focus on the heat balance first. The salt balance follows analogously. The conservation equation for temperature links the warming and cooling of water to advective and diffusive fluxes by

$$\frac{\partial T}{\partial t} = -\left(u\frac{\partial T}{\partial x} + v\frac{\partial T}{\partial y} + w\frac{\partial T}{\partial z}\right) - \left(\frac{\partial F_{Tx}}{\partial x} + \frac{\partial F_{Ty}}{\partial y} + \frac{\partial F_{Tz}}{\partial z}\right) \quad (5)$$

Here, t (s) is time, u, v, and w (m s^{-1}) are the components of the fluid velocity in x, y, and z direction, respectively, and F_{Tx}, F_{Ty}, and F_{Tz} (K m s^{-1}) are the three components of the diffusive temperature fluxes, respectively. We then simplify Eq. 5 to

$$\frac{\partial T}{\partial t} = TH - w\frac{\partial T}{\partial z} - \frac{\partial F_{Tz}}{\partial z} \quad (6)$$

where

$$TH = -\left(u\frac{\partial T}{\partial x} + v\frac{\partial T}{\partial y}\right) - \left(\frac{\partial F_{Tx}}{\partial x} + \frac{\partial F_{Ty}}{\partial y}\right) \quad (7)$$

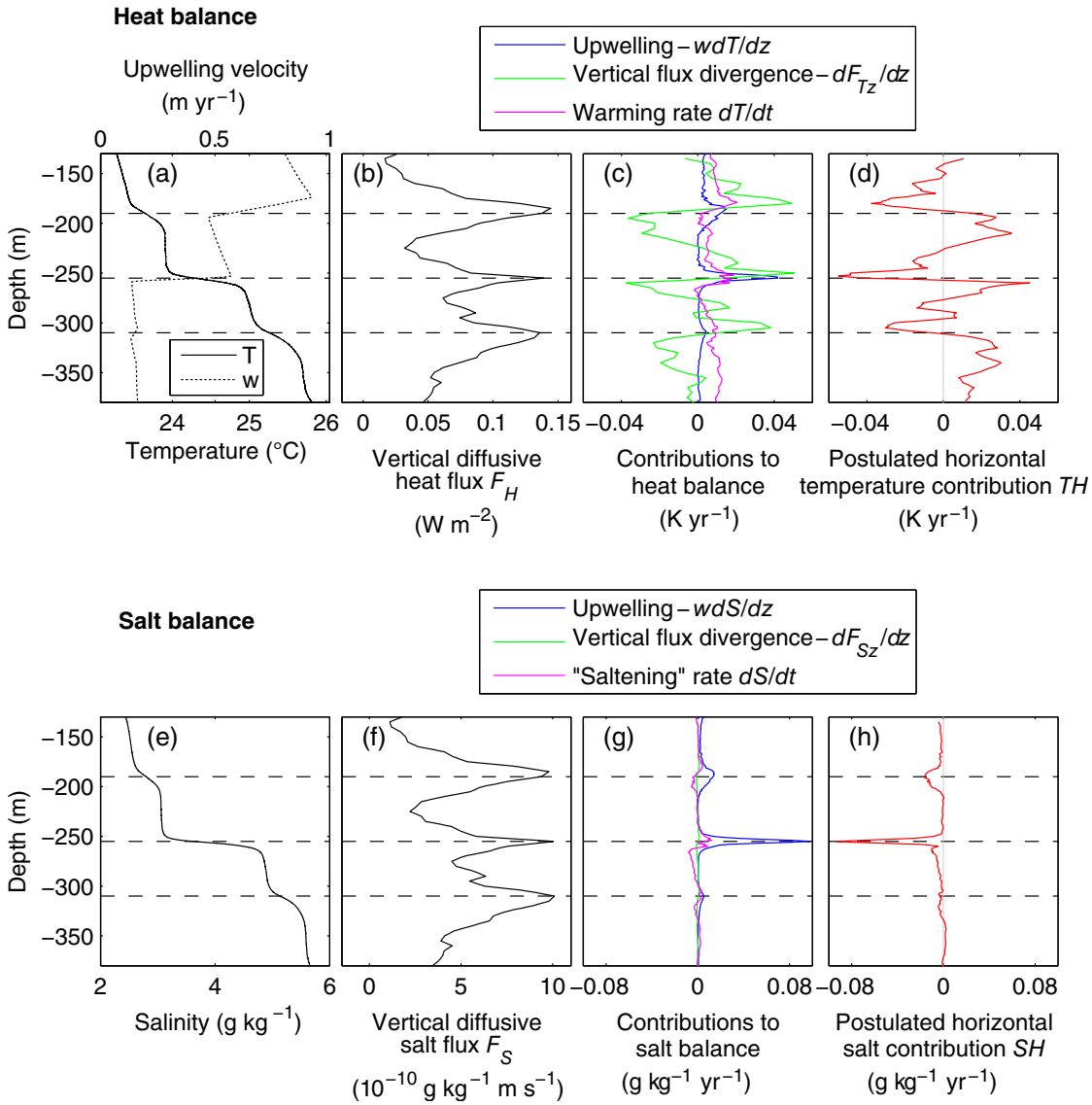

Fig. 5. Heat and salt balance. **(a)** Background temperature profile and upwelling velocity. The background temperature profile was calculated by averaging all 18 profiles marked blue and red in Fig. 1c. **(b)** Vertical diffusive heat flux, calculated from molecular fluxes through double-diffusive interfaces (identical to Fig. 4c). **(c)** Heat balance contributions, calculated directly from the data shown in **(a, b)**; **(d)** postulated horizontal temperature contribution to close the heat balance. **(e–h)** Same as **(a–d)**, but for salt. The horizontal dashed lines indicate the depths of the three major density gradients.

stands for the four horizontal temperature terms in x and y directions.

From the average temperature profile in Lake Kivu (Fig. 5a) and using the upwelling velocities from the model of Schmid et al. (2005) (Figs. 5a, 1b), we calculate the upwelling term $-w\partial T/\partial z$ of the heat balance (Fig. 5c, blue). If upwelling were the only temperature-changing process in Lake Kivu, the water would warm by ~ 40 mK yr^{-1} at 255 m depth and by ~ 10 mK yr^{-1} at 190 m depth, and thus partly exceed the observed warming rates (magenta in Fig. 5c). However, in the low gradient zones (e.g., at 225 and 350 m depth), upwelling is not sufficient to explain the observed warming.

As the vertical diffusive heat flux varies with depth (Figs. 5b, 4c), the vertical variation of the vertical diffusive heat flux $\partial F_{Tz}/\partial z$ (called vertical flux divergence in the legend of Fig. 5c) contributes to the heat balance. This contribution causes cooling below the three main gradients and warming above, thus acts to weaken the temperature gradients. Surprisingly, these warming and cooling rates, based on the vertical divergence of $\partial F_{Tz}/\partial z$, are much larger than both, the upwelling term and the observed warming rates.

To close the heat balance, we postulate the horizontal term TH (Fig. 5d, Eq. 7). This term is approximately the opposite of the diffusive flux contribution. It supplies cool water above the gradients and warm water below the gradients and thus

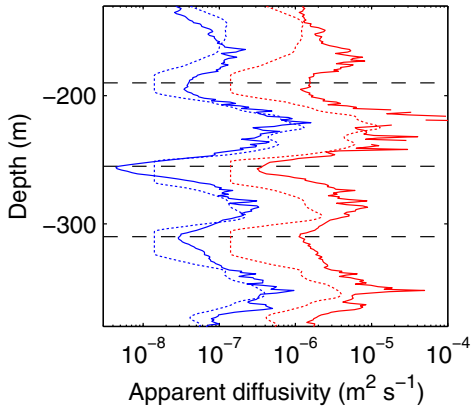

Fig. 6. Apparent diffusivities of temperature and salinity. Comparison of the apparent diffusivities estimated from our Lake Kivu data set (solid lines) and used in the model of Schmid et al. (2005) (dashed lines) for salinity (blue) and temperature (red). The depths of the three main gradients are indicated by horizontal dashed lines. Apparent diffusivities were calculated as described in Dissipation Rates of Turbulent Kinetic Energy section.

prevents the gradients from weakening over time. Recently, warm temperature anomalies below all main gradients and cold temperature anomalies above the 255 and 190 m gradients were reported in temperature profiles (Ross et al. 2015) thus supporting our hypothesis. Conversely, this implies that the subaquatic sources have a direct effect on the double-diffusive layering observed. In a long-term equilibrium, the steepness of the main gradients depends on the ratio between the upwelling rate and the diffusive transport. Stronger upwelling sharpens the gradients, while stronger diffusive transport weakens them. Without double diffusion, the main temperature gradients would thus be sharper than they are today. Between 1974 and 2010, a sharpening of the density gradients had been observed, which might have been caused by an increase in groundwater discharge (Schmid et al. 2012).

In the salt balance (Fig. 5e–h), the upwelling term dominates over the vertical diffusive flux. The horizontal contribution *SH* (defined as for temperature in Eq. 7) thus mainly supplies freshwater to the main gradients to compensate for the upwelling (Fig. 5f) as assumed in the model of Schmid et al. (2005).

The model of Schmid et al. (2005) assumed cold sources located only at the centers of the gradients. This was sufficient to balance the warming rates caused by upwelling. In the model, the vertical diffusive heat fluxes and the corresponding flux divergences were small. In Fig. 6, we compared the apparent diffusivities derived from our measurements to the ones used in Schmid et al. (2005). For temperature, the apparent diffusivities of the model are smaller than the measured ones by factors of 2 to 20 with the largest differences observed at the main gradients. For salinity, the apparent diffusivities of the model are smaller by factors 2 to 3 than the measured apparent diffusivities within the gradients at 190 and 310 m depth, but agree well with the measured apparent diffusivities over the remaining depth range.

We conclude that the subaquatic sources are responsible for the evolvement of double diffusion in Lake Kivu. The most important element for double diffusion to develop is the vertical structure of temperature and salinity shaped by the subaquatic sources, which provides the overall favorable background density ratio over the entire permanently stratified deep water for over hundreds of years. The enhanced vertical fluxes of heat induced by double-diffusive convection increase the transport of heat from the deep layers to the upper hypolimnion. This process would stop within a time scale of several decades without the local supply of heat from the subaquatic sources. Our observations of coherent layering in 2011 and 2015 in two depth intervals at 190 and 310 m depth indicate that the vertical structure of the double-diffusive layering can be maintained over several years within a water column that is slowly upwelling by a few decimeters per year. In order to study the underlying mechanism, individual layers have to be repeatedly monitored at time intervals smaller than the time scale given by the layer thickness over the upwelling velocity, which is approximately 0.5 m over 0.5 m yr^{-1}, thus 1 yr. Our measurements in 2011 and 2015 with a time difference of 4 yr are thus too coarse. We therefore cannot assess the movement, formation, and merging of individual double-diffusive layers within the rising water column.

Conclusion

We have presented a unique data set of 315 microstructure profiles covering almost the entire deep part of Lake Kivu on the Rwandese as well as on the Congolese side. Comparison of temperature profiles measured in 2011 and in 2015 showed that Lake Kivu has been warming at a rate of 8.6 mK yr^{-1} below 80 m depth. In the deep water at 350 m depth, a recent warming of ~ 10 mK yr^{-1} was observed that should be monitored in the future. The double-diffusive layering was shown to be present over most of the northern basin of Lake Kivu and, and at ~ 310 m depth, lateral coherency extended ~ 20 km into the south-eastern basin. Some layers measured in 2011 could be identified again in 2015, indicating extremely small temporal variability, slow layer evolution, and large lateral coherency in those particular layers. Temperature maps created from coherent layers revealed cold intrusions from the northern shore at a depth of 190 m. Estimates of dissipation of turbulent kinetic energy, based on 29.6% of the measured microstructure segments, revealed an average of 1.5×10^{-10} W kg^{-1}. Assuming that the other 70.4% of the unshaped Batchelor spectra were caused by too weak turbulence (with dissipation rate = 0) provides a mixed layer dissipation average of 0.44×10^{-10} W kg^{-1}, corresponding to a vertical diffusive heat flux of 0.10 W m^{-2}. The same average value resulted from independent measurements of the molecular heat fluxes through the double-diffusive interfaces. The largest vertical diffusive fluxes were observed in the main gradients at 190, 255, and 310 m depth. To close the heat and

salt balance, we postulate horizontal contributions. To close the salinity balance, horizontal inputs of freshwater are required at the main gradients to balance upwelling. For heat, we require an input of cold water above the main gradients and warm water below those gradients. As the effect of the horizontal inputs of warm and cold water is approximately inverse to the effect of double diffusion in the heat and salt balance, we suggest that the subaquatic sources are responsible for the evolvement of double diffusion in Lake Kivu.

In this work, we have shown that information on double-diffusive staircases can contribute to the understanding of a water body as a whole. For Lake Kivu, the long-ranging horizontal coherence of double-diffusive layering suggests small horizontal variability, justifying one-dimensional lake models. For future models, we suggest to consider (i) the observed warming of the lake, (ii) the measured apparent diffusivities, and (iii) the estimated horizontal contributions to the budget of heat and salt.

References

Batchelor, G. K. 1959. Small-scale variation of convected quantities like temperature in turbulent fluid. Part 1. General discussion and the case of small conductivity. J. Fluid Mech. **5**: 113–133. doi:10.1017/S002211205900009X

Fey, A., and R. Conrad. 2000. Effect of temperature on carbon and electron flow and on the archaeal community in methanogenic rice field soil. Appl. Environ. Microbiol. **66**: 4790–4797. doi:10.1128/AEM.66.11.4790-4797.2000

Gayen, B., G. O. Hughes, and R. W. Griffiths. 2013. Completing the mechanical energy pathways in turbulent Rayleigh-Bénard convection. Phys. Rev. Lett. **111**: 124301. doi:10.1103/PhysRevLett.111.124301

Gibson, C. H., and W. H. Schwarz. 1963. The universal equilibrium spectra of turbulent velocity and scalar fields. J. Fluid Mech. **16**: 365–384. doi:10.1017/S0022112063000835

Gregg, M. C., E. A. D'Asaro, J. J. Riley, and E. Kunze. 2018. Mixing efficiency in the ocean. Ann. Rev. Mar. Sci. **10**: 443–473. doi:10.1146/annurev-marine-121916-063643

Griffiths, R. 1979. The transport of multiple components through thermohaline diffusive interfaces. Deep-Sea Res. **26A**: 383–397. doi:10.1016/0198-0149(79)90052-9

Hieronymus, M., and J. R. Carpenter. 2016. Energy and variance budgets of a diffusive staircase with implications for heat flux scaling. J. Phys. Oceanogr. **46**: 2553–2569. doi:10.1175/JPO-D-15-0155.1

Katsev, S., A. A. Aaberg, S. A. Crowe, and R. E. Hecky. 2014. Recent warming of Lake Kivu. PLoS One **9**: e109084. doi:10.1371/journal.pone.0109084

Kelley, D. E., H. J. S. Fernando, A. E. Gargett, J. Tanny, and E. Özsoy. 2003. The diffusive regime of double-diffusive convection. Prog. Oceanogr. **56**: 461–481. doi:10.1016/S0079-6611(03)00026-0

Kocsis, O., H. Prandke, A. Stips, A. Simon, and A. Wüest. 1999. Comparison of dissipation of turbulent kinetic energy determined from shear and temperature microstructure. J. Mar. Systems **21**: 67–84. doi:10.1016/S0924-7963(99)00006-8

Kunze, E. 2003. A review of oceanic salt-fingering theory. Prog. Oceanogr. **56**: 399–417. doi:10.1016/S0079-6611(03)00027-2

Lorke, A., K. Tietze, M. Halbwachs, and A. Wüest. 2004. Response of Lake Kivu stratification to lava inflow and climate warming. Limnol. Oceanogr. **49**: 778–783. doi:10.4319/lo.2004.49.3.0778

Meccia, V. L., S. Simoncelli, and S. Sparnocchia. 2016. Decadal variability of the turner angle in the Mediterranean Sea and its implications for double diffusion. Deep-Sea Res. Part I Oceanogr. Res. Pap. **114**: 64–77. doi:10.1016/j.dsr.2016.04.001

Muvundja, F. A., A. Wüest, M. Isumbisho, B. M. Kaningini, N. Pasche, P. Rinta, and M. Schmid. 2014. Modelling Lake Kivu water level variations over the last seven decades. Limnologica **47**: 21–33. doi:10.1016/j.limno.2014.02.003

O'Reilly, C. M., S. R. Alin, P.-D. Plisnier, A. S. Cohen, and B. A. McKee. 2003. Climate change decreases aquatic ecosystem productivity of Lake Tanganyika, Africa. Nature **424**: 766–768. doi:10.1038/nature01833

Pasche, N., M. Schmid, F. Vazquez, C. J. Schubert, A. Wüest, J. D. Kessler, M. A. Pack, W. S. Reeburgh, and H. Bürgmann. 2011. Methane sources and sinks in Lake Kivu. J. Geophys. Res. **116**: G03006. doi:10.1029/2011JG001690

Polyakov, I. V., A. V. Pnyushkov, R. Rember, V. V. Ivanov, Y.-D. Lenn, L. Padman, and E. C. Carmack. 2012. Mooring-based observations of double-diffusive staircases over the Laptev Sea slope. J. Phys. Oceanogr. **42**: 95–109. doi:10.1175/2011JPO4606.1

Radko, T. 2013. Double-diffusive convection. Cambridge Univ. Press. doi:10.1017/CBO9781139034173

Ross, K. A., E. Gashugi, A. Gafasi, A. Wüest, and M. Schmid. 2015. Characterisation of the subaquatic groundwater discharge that maintains the permanent stratification within Lake Kivu; East Africa. PLoS One **10**: e0121217. doi:10.1371/journal.pone.0121217

Ruddick, B., A. Anis, and K. Thompson. 2000. Maximum likelihood spectral fitting: The Batchelor spectrum. J. Atmos. Oceanic Tech. **17**: 1541–1555. doi:10.1175/1520-0426(2000)017<1541:MLSFTB>2.0.CO;2

Scheifele, B., R. Pawlowicz, T. Sommer, and A. Wüest. 2014. Double diffusion in saline Powell Lake, British Columbia. J. Phys. Oceanogr. **44**: 2893–2908. doi:10.1175/JPO-D-14-0070.1

Schmid, M., K. Tietze, M. Halbwachs, A. Lorke, D. McGinnis, and A. Wüest. 2003. How hazardous is the gas accumulation in Lake Kivu? Arguments for a risk assessment in light of the Nyiragongo volcano eruption of 2002. Acta Vulcanol. **14**: 115–122. doi:10.1400/19084

Schmid, M., A. Lorke, C. Dinkel, G. Tanyileke, and A. Wüest. 2004. Double-diffusive convection in Lake Nyos Cameroon.

Deep-Sea Res. Part I Oceanogr. Res. Pap. **51**: 1097–1111. doi:10.1016/j.dsr.2004.02.010

Schmid, M., M. Halbwachs, B. Wehrli, and A. Wüest. 2005. Weak mixing in Lake Kivu: New insights indicate increasing risk of uncontrolled gas eruption. Geochem. Geophys. Geosyst. **6**: Q07009. doi:10.1029/2004GC000892

Schmid, M., M. Busbridge, and A. Wüest. 2010. Double-diffusive convection in Lake Kivu. Limnol. Oceanogr. **55**: 225–238. doi:10.4319/lo.2010.55.1.0225

Schmid, M., and A. Wüest. 2012. Stratification, mixing and transport processes in Lake Kivu, p. 13–29. *In* J.-P. Descy, F. Darchambeau, and M. Schmid [eds.], Lake Kivu: Limnology and biogeochemistry of a tropical great Lake. Springer Science. doi:10.1007/978-94-007-4243-7_2

Schmid, M., K. A. Ross, and A. Wüest. 2012. Comment on An additional challenge of Lake Kivu in Central Africa—upward movement of the chemoclines by Finn Hirslund. J. Limnol. **71**: 330–334. doi:10.4081/jlimnol.2012.e35

Schmitt, R. W. 1994. Double diffusion in oceanography. Annu. Rev. Fluid Mech. **26**: 255–285. doi:10.1146/annurev.fl.26.010194.001351

Schmitt, R. W. 2003. Observational and laboratory insights into salt finger convection. Prog. Oceanogr. **56**: 419–433. doi:10.1016/S0079-6611(03)00033-8

Schmitt, R. W., H. Perkins, J. D. Boyd, and M. C. Stalcup. 1987. C-SALT: An investigation of the thermohaline staircase in the western tropical North Atlantic. Deep Sea Res. Part A. Oceanogr. Res. Pap. **34**: 1655–1665. doi:10.1016/0198-0149(87)90014-8

Sommer, T., J. R. Carpenter, M. Schmid, R. G. Lueck, M. Schurter, and A. Wüest. 2013*a*. Interface structure and flux laws in a natural double-diffusive layering. J. Geophys. Res. Ocean. **118**: 6092–6106. doi:10.1002/2013JC009166

Sommer, T., J. R. Carpenter, M. Schmid, R. G. Lueck, and A. Wüest. 2013*b*. Revisiting microstructure sensor responses with implications for double-diffusive fluxes. J. Atmos. Oceanic Tech. **30**: 1907–1923. doi:10.1175/JTECH-D-12-00272.1

Sommer, T., J. R. Carpenter, and A. Wüest. 2014. Double-diffusive interfaces in Lake Kivu reproduced by direct numerical simulations. Geophys. Res. Lett. **41**: 5114–5121. doi:10.1002/2014GL060716

Steinbuck, J. V., M. T. Stacey, M. A. McManus, O. M. Cheriton, and J. P. Ryan. 2009*a*. Observations of turbulent mixing in a phytoplankton thin layer: Implications for formation, maintenance, and breakdown. Limnol. Oceanogr. **54**: 1353–1368. doi:10.4319/lo.2009.54.4.1353

Steinbuck, J. V., M. T. Stacey, and S. G. Monismith. 2009*b*. An evaluation of χ_T estimation techniques: Implications for Batchelor fitting and ε. J. Atmos. Oceanic Tech. **26**: 1652–1662. doi:10.1175/2009JTECHO611.1

Timmermans, M.-L., J. Toole, R. Krishfield, and P. Winsor. 2008. Ice-tethered profiler observations of the double-diffusive staircase in the Canada Basin thermocline. J. Geophys. Res. **113**: C00A02. doi:10.1029/2008JC004829

Toffolon, M., A. Wüest, and T. Sommer. 2015. Minimal model for double diffusion and its application to Kivu, Nyos, and Powell Lake. J. Geophys. Res. Ocean. **120**: 6202–6224. doi:10.1002/2015JC010970

Verburg, P., R. E. Hecky, and H. Kling. 2003. Ecological consequences of a century of warming in Lake Tanganyika. Science **301**: 505–507. doi:10.1126/science.1084846

Acknowledgments

The authors thank Georges Alunga, Patrick Habakaramo, Pascal Isumbisho Mwapu, Katcho Karume, Fabrice Muvundja, and Augusta Umutoni for local support during field work, Barry Ruddick and Jeffrey Carpenter for providing code for Batchelor fitting, Magnus Hieronymus and Jeffrey Carpenter for discussions on the heat and salt balance, Rolf Lück for support with the microstructure profiler, and Rich Pawlowicz for providing the Matlab code used for the maps in Figs. 1, 3. This work was financed by the Swiss National Science Foundation—200021-122183 and 200020–140538 (Lake Kivu - turbulence and double diffusion in permanent stratification). The authors want to dedicate this publication to Michael Schurter, who deceased recently while preparing the revisions of this manuscript. With his technical expertise, his careful management of the logistics, his strong and constant commitment, and his open and friendly communication with the local partners, he was a cornerstone for the success of the many field measurement campaigns and he contributed to the great progress in the understanding of the functioning of Lake Kivu.

Conflict of Interest

None declared.

Submitted 05 February 2018
Revised 11 June 2018 and 25 September 2018
Accepted 02 October 2018

Associate editor: Leon Boegman